Determination of the Fracture Toughness of Glasses via Scratch Tests with a Vickers Indenter

Haitao Liu[1]   Jianwei Zhang[1,2]⋆   Minghao Zhao[1,2,3]⋆   Chunsheng Lu[4]

([1]*School of Mechanics and Safety Engineering, Zhengzhou University, Zhengzhou 450001, China*)

([2]*School of Mechanical and Power Engineering, Zhengzhou University, Zhengzhou 450001, China*)

([3]*Henan Key Engineering Laboratory for Anti-fatigue Manufacturing Technology, Zhengzhou 450001, China*)

([4]*School of Civil and Mechanical Engineering, Curtin University, Perth 6845, Western Australia, Australia*)

ABSTRACT Fracture toughness is an important index in safety evaluation for materials and structures. Its convenient and accurate characterization has attracted extensive attention. For small specimens, traditional testing methods of fracture toughness are not suitable due to limitations in sample size and shape. In this work, a new formula is proposed to determine the fracture toughness of glasses using scratch tests with a Vickers indenter based on dimensional analysis and finite element analysis. Fracture toughness of glasses could be calculated with elastic modulus, crack depth of scratched materials and normal force applied during the scratch tests. The effects of plastic deformation and interfacial friction between the Vickers indenter and scratched materials are considered, and the crack shape is consistent with experimental observations. The proposed formula is verified by comparing the fracture toughness of soda-lime and borosilicate glasses obtained from scratch tests with those obtained via indentation tests. This work provides an alternative method to determine the fracture toughness of glass materials.

KEY WORDS Scratch test, Fracture toughness, Glass, Dimensional analysis, Finite element analysis

1. Introduction

As an index for characterizing crack propagation resistance, fracture toughness is one of the most important material parameters of engineering materials, including glass [1–3]. The single-edge-notched beam and compact tension methods are frequently used to determine the fracture toughness of engineering materials [4–6]. However, owing to the high cost and inconvenience of preparing standard specimens for these methods, the indentation and scratch methods have been developed to characterize the fracture toughness of engineering materials [7–9].

The convenience of performing the indentation test has made it a widely used method to determine the fracture toughness of brittle materials [10–12]. Using a Vickers indenter, Evans and Charles [13] proposed an empirical formula to relate the fracture toughness of materials to the crack length under an indentation load with the condition that the crack length is much larger than the half diagonal of the impression. Based on the analysis of stress field and crack evolution during indentation tests, Lawn et al. [14] obtained an expression to determine the fracture toughness of ceramics. Furthermore, Feng

---

⋆ Corresponding authors. E-mails: zhangjianwei@zzu.edu.cn; memhzhao@zzu.edu.cn

et al. [15] developed an indentation method to estimate fracture toughness based on loading work. Feng et al. [16] and Ostojic et al. [17] made detailed reviews on determining fracture toughness of brittle materials via the indentation method.

In addition to studying the wear behaviors of polymeric materials [18–20] and interfacial adhesion between film and substrate [21], the scratch test has also been used to determine the fracture toughness of materials [22–24]. Analyzing the scratch results of ceramics, Subhash et al. [25] proposed a new brittle measurement based on the ratio of the energy contained in the driving frequency to the total energy in the spectrum. Cook [26] performed a complete theoretical and experimental analysis of scratch damage by a Vickers indenter to investigate the strength of polycrystalline alumina containing controlled scratches. Liu et al. [27] investigated the fracture properties of a surface modification layer with a modified bi-layer beam model for scratch tests. Neglecting the effects of plastic deformation and interfacial friction, Akono et al. [28, 29] adopted the scratch test to determine the fracture toughness of engineering materials. However, Lin and Zhou [30] argued that the assumptions made for the crack location and contact condition between the scratch probe and scratched materials in the work of Akono et al. [28, 29] may not be appropriate. Liu et al. [31, 32] used Rockwell C diamond indenter to investigate the scratch behaviors of copper and polycarbonate under continuous loading and determine their fracture toughness through scratch tests. Using finite element simulation and dimensional analysis, Liu et al. [33] proposed two concise formulas to characterize the yield stress of glass and the interfacial coefficient of friction between scratch tip and glass. However, the scratch-induced cracks were not considered in the work of Liu et al. [33] and thus, fracture toughness cannot be determined .

In this paper, a formula based on finite element simulation and dimensional analysis is proposed to determine the fracture toughness of glass via scratch tests with a Vickers indenter. The crack shape refers to the experimental observations of glasses in the process of obtaining the formula, and the effects of plastic deformation and interfacial friction are also considered. The paper is organized as follows: Sect. 2 introduces the formula obtained from the finite element and dimensional analysis, and Sect. 3 describes the experimental verification of the formula on soda-lime and borosilicate glasses. Finally, conclusions are drawn in Sect. 4.

2. Method Development

The scratch process of a brittle material such as glass with a Vickers indenter under linearly increasing normal load can be divided into three stages according to the deformation and failure mode, i.e., micro-ductile regime, micro-cracking regime and micro-abrasive regime [34, 35], as shown in Fig. 1. Elastic-plastic deformation dominates in the stage of micro-ductile regime, and no crack occurs. In the second stage, a median crack can be observed in the early stage of micro-cracking regime. As the normal force increases, lateral crack occurs. Microfracture chips can be observed in the stage of micro-abrasive regime [33]. Since the critical load for crack initiation of median crack is lower than that of lateral crack [36], a median crack without lateral cracks and microfracture chips can be observed along the scratch path within a specific normal load range according to the mechanical properties of scratched materials in the second stage. Figure 2a shows a schematic plot of a scratch test using a Vickers indenter under a constant normal load, which could be classified into the second stage. Figure 2b shows the longitudinal section of such a scratch-induced crack. The shape of the crack front is assumed to be an ellipse with a major radius R_a and a minor radius R_b, as shown in Fig. 2b. The parameter R_b can also be described as the crack depth.

For a steady scratch test under a constant normal load, the corresponding scratch depth is constant. Thus, the normal load does not do work in the scratch process. Only the tangential force F_t does work. In the scratch process, elastic deformation stores energy, while plastic deformation and friction work consume energy. The rest of the work is consumed to create new crack surfaces in this scratch test with a crack. From the viewpoint of energy conservation, the energy consumed by crack propagation $G\left(R_b l + \pi R_a R_b/4\right)$ equals the total energy input, $F_t l$, subtracting the elastic energy restored ΔW_e, the energy dissipation during the scratch process (i.e., the plastic energy) ΔW_p and the work consumed by interfacial friction ΔW_f. The specific expression is given as

$$G\left(R_b l + \pi R_a R_b/4\right) = F_t l - \Delta W_e - \Delta W_p - \Delta W_f \tag{1}$$
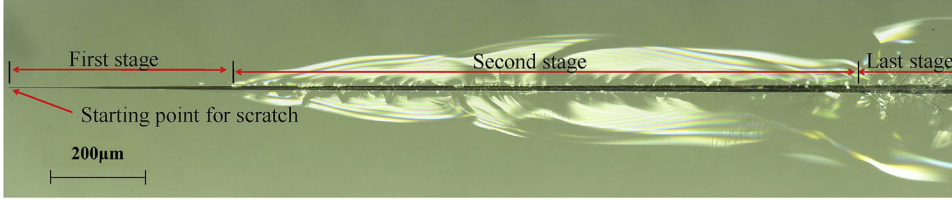
Fig. 1. Three stages during the scratch process of soda-lime glass with a Vickers indenter under a linearly increasing normal load. First stage: micro-ductile regime, Second stage: micro-cracking regime and Last stage: micro-abrasive regime [33]
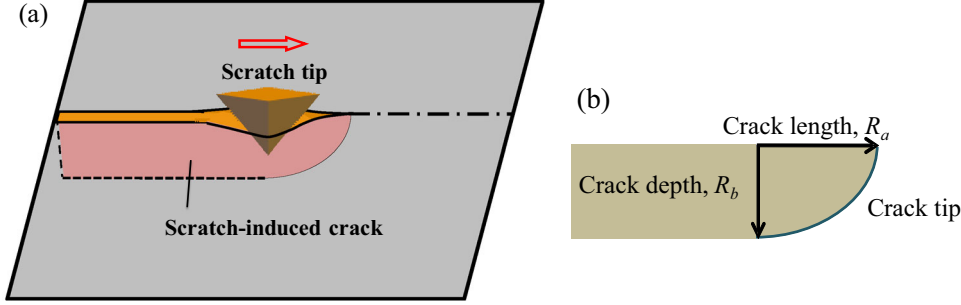

Fig. 2. Schematics of a **a** scratch test with a Vickers indenter under a constant normal load; **b** scratch-induced crack

where l is the moving distance of the Vickers indenter. For the steady-state crack growth, l equals the crack propagation distance. R_a and R_b are constants. Eq. (1) could be rewritten as follows.

$$G = (F_t l - \Delta W_e - \Delta W_p - \Delta W_f)/(R_b l + \pi R_a R_b/4) \tag{2}$$

Due to the brittleness of scratched material, the crack size is far larger than the size of yield area. Under linear elastic fracture mechanics, the relationship between the stress intensity factor, K_I, and the energy release rate, G, can be represented as

$$K_I = \sqrt{EG} = \sqrt{E\left(F_t l - \Delta W_e - \Delta W_p - \Delta W_f\right)/\left(R_b l + \pi R_a R_b/4\right)} \tag{3}$$

It should be noted that it is impractical to determine ΔW_e, ΔW_p and ΔW_f from the scratch test. Dimensional analysis and finite element analysis are used to determine these values and then obtain a formula to characterize the fracture toughness of brittle materials.

2.1. Dimensional Analysis

In the scratch test, the normal force and scratch velocity should be given. For the condition that the scratch velocity is sufficiently small, the scratch progress can be viewed as a quasi-static state. For simplicity, the effect of indenter shape on the scratch results is not considered. Here, a Vickers indenter is adopted. The ideal elastic-plastic constitutive relation, as characterized by the elastic modulus (E), Poisson's ratio (v) and yield stress (σ_s), was adopted to describe the mechanical properties of scratched materials. In the scratch test with a crack, material properties (E, v, and σ_s), external load (F_n), crack geometry (R_a and R_b) and interfacial coefficient of friction (μ_s) may have effects on the stress intensity factor (K_I), as shown in Eq. (4).

$$K_I = f\left(E, v, \sigma_s, F_n, R_a, R_b, \mu_s\right) \tag{4}$$

Applying the π-theorem and choosing E and R_b as independent variables, other parameters could be expressed as $[K_I] = [\sigma_s][R_b]^{\frac{1}{2}} = \sqrt{[E][F_n]/[R_b]}$, $[E] = [\sigma_s][R_b]^0$, $[\nu] = [\mu_s] = [\sigma_s]^0[R_b]^0$, $[F_n] = [\sigma_s][R_b]^2$, and $[R_a] = [\sigma_s]^0[R_b]$. The effect of Poisson's ratio on K_I can be neglected because its effect on the stress intensity factor is not apparent [37, 38]. Eq. (4) can be expressed in a dimensionless form as
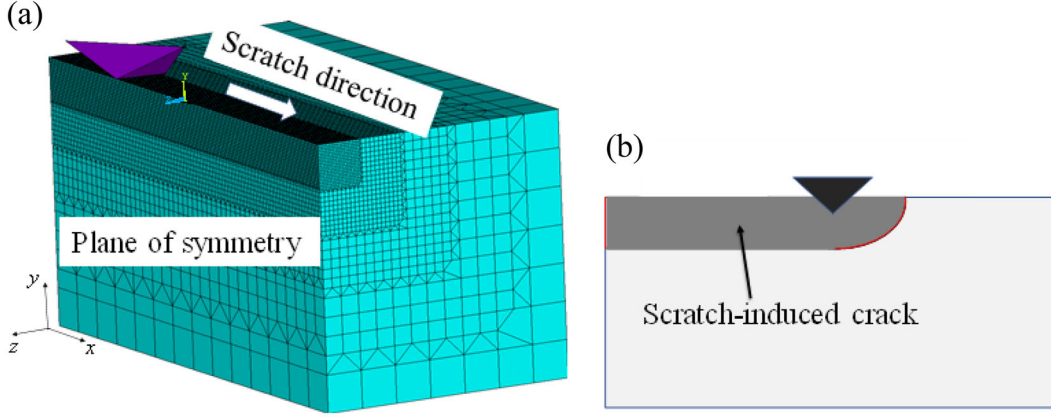
(a)

(b)

Fig. 3. **a** Finite element model of a scratch test with a Vickers indenter; **b** schematic of plane of symmetry

$$\frac{K_I}{\sqrt{EF_n/R_b}} = \mathcal{F}\left(\frac{\sigma_s}{E}, \frac{R_a}{R_b}, \mu_s\right) \tag{5}$$

The specific form of Eq. (5) will be investigated according to the finite element results.

2.2. Finite Element Simulation

2.2.1. Finite Element Model

Figure 3a shows the 3D finite element model used to simulate the scratch process. Considering symmetry, a half model with the dimension of 224 μm × 112 μm × 112 μm was created in the commercial finite element software Ansys R18.0. Solid186 element was adopted for the scratched material. Only the elements along the scratch path were refined to improve computational efficiency. A minimum mesh size of 1 μm × 1 μm × 1 μm was utilized. The Vickers indenter with a face angle of 136° was modeled as a rigid body. The TARGET170 and CONTACT174 elements were used for the contact surfaces of the Vickers indenter and the scratched material. The freedoms in the y-direction at the bottom were constrained, so were the right and left sides in the x-direction. The freedoms in the z-direction of gray areas in the plane of symmetry were unconstrained because of the existence of the crack, while other areas were constrained, as shown in Fig. 3b. It should be noted that there is initial crack on the plane of symmetry of the scratched material before scratching in the simulation. R_a, R_b, and the distance between the crack tip and the Vickers indenter are kept unchanged during the scratch process by controlling the release of constraints of the nodes in the plane of symmetry according to their coordinates. The process is automatically executed by applying the if-statement using APDL (ANSYS Parametric Design Language). Thus, the crack shape can be modeled.

Plastic deformation exists in the scratch process of brittle materials, such as glass [34, 35]. According to Lacroix et al. [39], the compressed glass pillars in the microscale act like an elastic-perfectly plastic material. Thus, the ideal elastic-plastic constitutive relation was adopted. To cover the ranges of E and σ_s of the prepared glasses, the values of E used in the finite element simulations ranged from 50 to 200 GPa, and those of σ_s ranged from 200 to 1200 MPa. Poisson's ratio was set to 0.25. Corresponding to normal forces, constant normal scratch depths were applied on the scratch tip for the consideration of convergence. The scratch distance was 32 μm with a scratch velocity of 1 μm/s. The scratch depth varied from 0 to 20 μm, while the range of the interfacial coefficient of friction was from 0 to 0.1. Parameters used in the finite element simulation are shown in Table 1.

2.2.2. Finite Element Results

Figure 4 shows that an increase in the normal force F_n causes the stress intensity factor K_I, as calculated from Eq. (3), to increase remarkably. From Fig. 4a, elastic modulus has a significant effect on K_I. Figure 4b and d shows that the influences of yield stress and interfacial coefficient of friction on K_I are not obvious. Figure 4c indicates that the effect of R_b is much larger than R_a on K_I.

Table 1. **Parameters used in the finite element simulation**

Elastic modulus (GP_a)	Poisson's ratio	Yield stress (MP_a)	Scratch depth (μm)	Coefficient of friction	R_a (μm)	R_b (μm)
				0		
			2	0.01		
			4	0.02		
		200	6	0.03		
50		400	8	0.04	30	20
75		600	10	0.05	60	40
100	0.25	800	12	0.06	90	60
150		1000	14	0.07		
200		1200	16	0.08		
			18	0.09		
			20	0.1		

From Fig. 5a, the interfacial coefficient of friction has a significant effect on the normalized tangential force F_t/F_n. Because the normalized friction work $\Delta W_f/F_t l$ is almost proportional to the normalized tangential force, the increase in work owing to increasing the interfacial coefficient of friction is consumed in the form of friction work during the scratch test. As the friction work is subtracted in Eq. (3), the interfacial coefficient of friction has little effect on the stress intensity factor. From Fig. 5b, with the increase in interfacial coefficient of friction, the proportion of elastic energy, plastic energy and energy consumed to create new surfaces in total energy decrease, while the proportion of friction work in the total energy increases significantly. As the plastic energy and frictional energy account for a large proportion of the total energy, their effects on the scratch results could not be neglected. Using different cutters with different number of sidewalls, i.e., U-cut, L-cut and slab-cut, Lin and Zhou [40] suggested that sidewall friction during scratch test is substantial. This work also confirms that the friction work accounts for a large part of the total energy, especially for a large interfacial coefficient of friction. Its influence on the scratch responses cannot be ignored.

Figure 6 shows that the normalized stress intensity factor $K_I/\left(EF_n/R_b\right)^{0.5}$ is a nearly constant value for various values of F_n, E, R_b, σ_s and μ_s. A crack propagates if the stress intensity factor K_I reaches the critical stress intensity factor K_{Ic}. Based on the results above, the critical stress intensity factor can be expressed as

$$K_{Ic} = 0.31\sqrt{EF_n/R_b} \tag{6}$$

As R_b can be measured in the scratch test, E is a mechanical parameter of the scratched material and F_n is the applied normal load, K_{Ic} can be determined conveniently via scratch tests. It should be noted that, according to the assumption, the proposed formula is appropriate for a scratch test with a median crack located at the center of the scratch-induced groove.

3. Determining the Fracture Toughness of Glass Materials via Scratch Tests

3.1. Experimental Details

Soda-lime and borosilicate glasses were chosen to validate Eq. (6). In order to facilitate the observation of the scratch fracture phenomenon, the sample size was set as 30 mm× 80 mm× 3 mm. Using an optical profiler (Bruker NPFLEX), the surface roughness values of soda-lime and borosilicate glass were 11.09± 0.79 nm and 10.27± 1.46 nm, respectively. Using a nanoindentation instrument (Agilent Nano Indenter G200), the elastic moduli of soda-lime and borosilicate glasses were 63.60± 0.27 GPa and 79.13± 0.26 GPa, respectively. The Vickers hardness values of soda-lime and borosilicate glasses were 3.16± 0.15 GPa and 5.37± 0.24 GPa, respectively.

The scratch tests of the soda-lime and borosilicate glasses were performed on NANOVEA PB1000. The face angle of the diamond Vickers indenter was 136° . For the normal load, 0.2 N and 0.3 N were used for soda-lime and borosilicate glasses, respectively. The scratch velocity was 2 mm min^{-1}, and
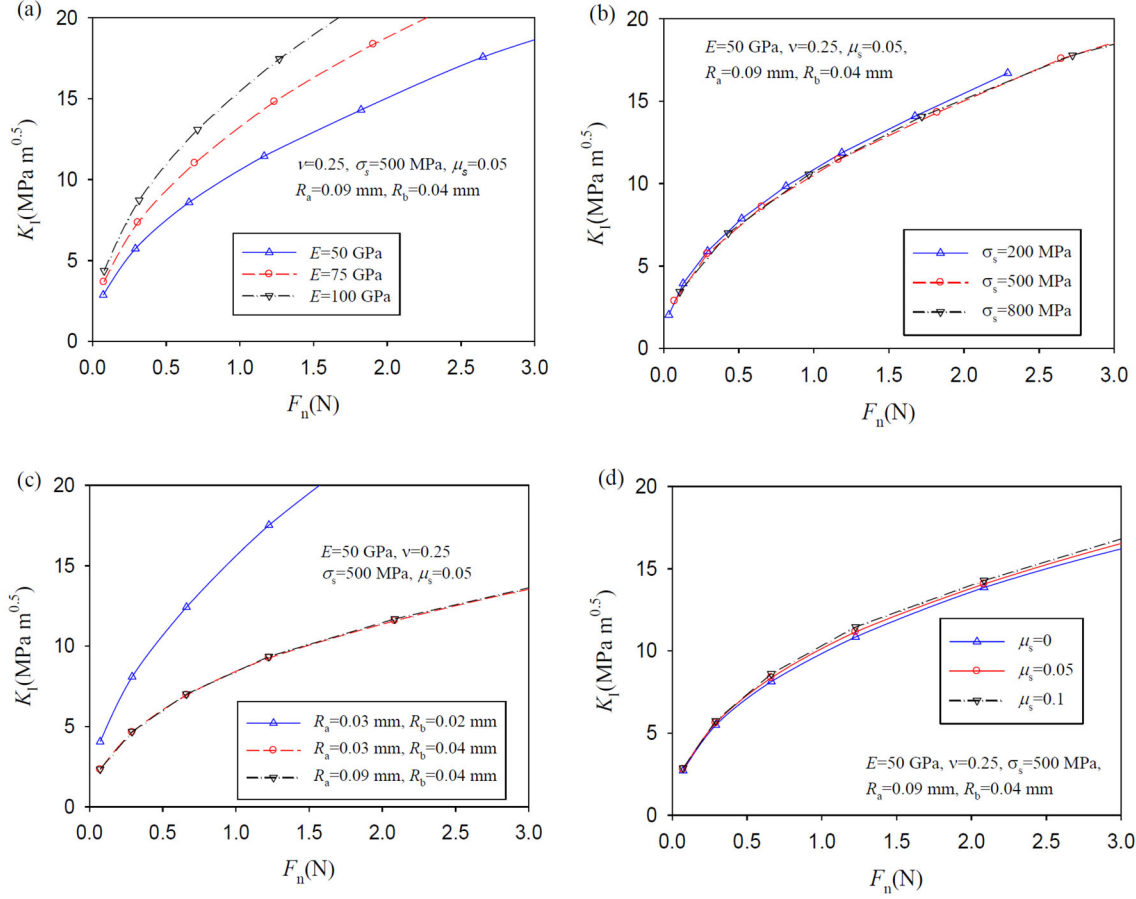
Fig. 4. The influences of **a** elastic modulus, **b** yield stress, **c** R_a, R_b, and **d** coefficient of friction on stress intensity factor

the scratch length was 5 mm to obtain a stable scratch state. All of the scratch tests were performed at room temperature. Five identical tests were performed for each scratch test condition.

To verify the fracture toughness of glasses as determined by the scratch test, indentation tests of the two glass specimen types were also performed by the mechanical tester (NANOVEA PB1000) with a diamond Vickers indenter. In these tests, a loading rate of 8 N/min was used, where the maximum indentation load was 4 N. Five identical tests were performed for each indentation test condition.

To assess the surface damage features and to measure the crack length, the scratched and indented glasses were optically scanned by a confocal laser scanning microscope (KEYENCE VHX-2000).

3.2. Results and Discussion

Figure 7 shows the results of scratch tests of soda-lime glass under a constant load of 0.2 N. From the top view (Fig. 7a) and a longitudinal section of the crack along the scratch path (Fig. 7b), there exists a scratch-induced crack in the scratch tests, which is consistent with the assumption regarding the shape of crack in the finite element simulation. R_b can be determined from the scratched samples as shown in Fig. 7b. The results of borosilicate glass are similar to that of soda-lime glass.

From Fig. 8, the fracture toughness of soda-lime and borosilicate glasses obtained from scratch tests is 0.74 ± 0.04 MPa$\sqrt{m}$ and 1.06 ± 0.09 MPa$\sqrt{m}$, respectively. To validate the fracture toughness values of glasses obtained from the scratch tests, the indentation method was also performed using the relation [41]

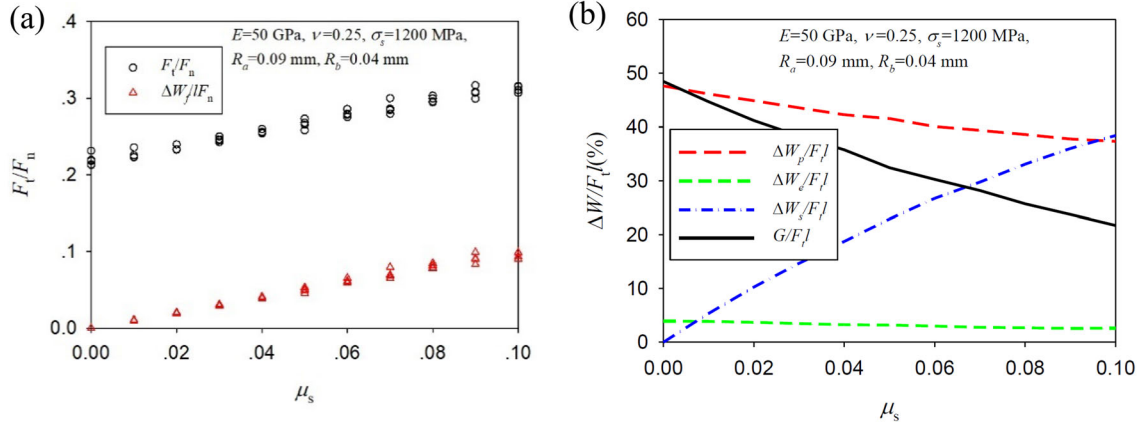$$K_c = \alpha \left(E/H \right)^{0.5} \left(P/c^{1.5} \right) \tag{7}$$

Fig. 5. The effect of interfacial coefficient of friction on **a** normalized tangential force and **b** normalized energy during scratch
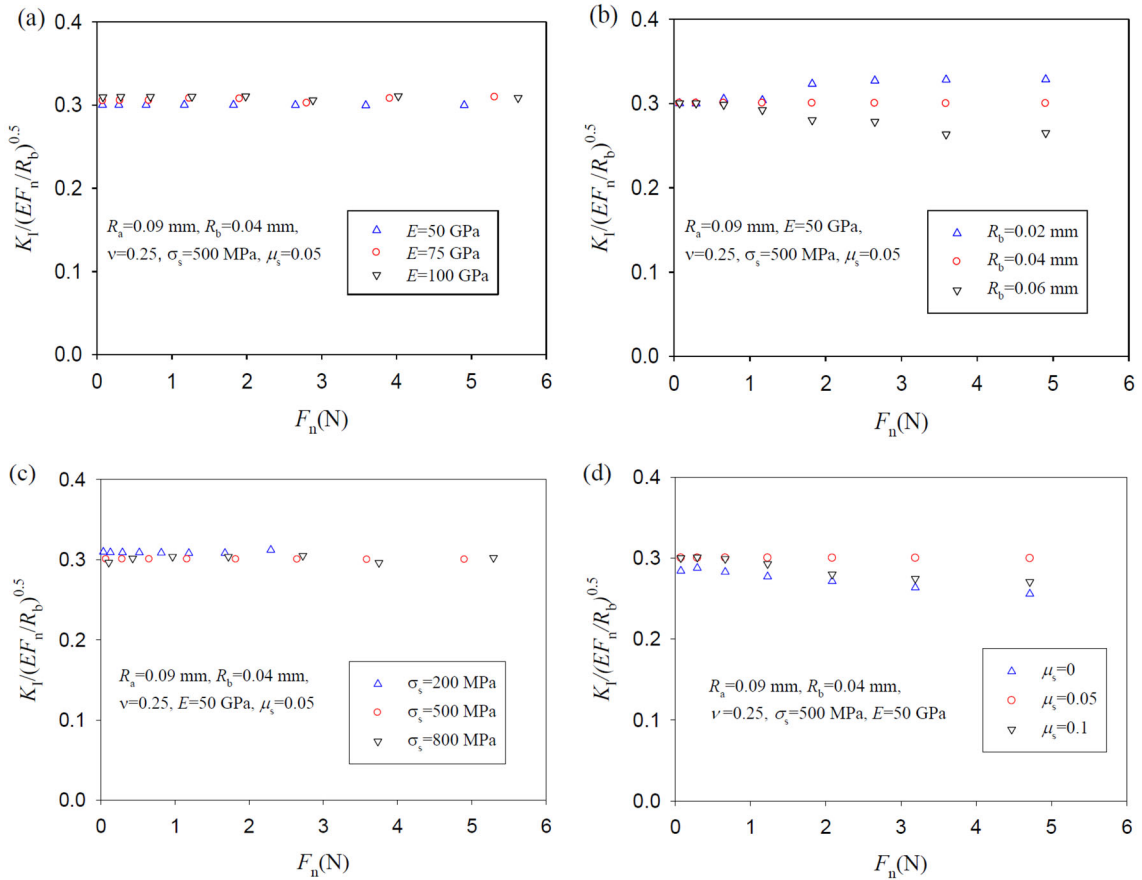

Fig. 6. The influences of **a** elastic modulus, **b** crack depth, **c** yield stress, and **d** coefficient of friction on normalized $K_{\rm I}$

where α is an empirical constant depending on the indenter geometry, H is hardness, and c is crack length. For a Vickers indenter, $\alpha = 0.016$ [41]. The fracture toughness values of soda-lime and borosilicate glasses determined by indentation tests are 0.71 ± 0.03 MPa$\sqrt{\rm m}$ and 1.15 ± 0.15 MPa$\sqrt{\rm m}$, respectively. The fracture toughness values of borosilicate and soda-lime glasses obtained from scratch tests are also similar to the results of Iwata et al. [42] and Gong et al. [43]. Besides soda-lime and
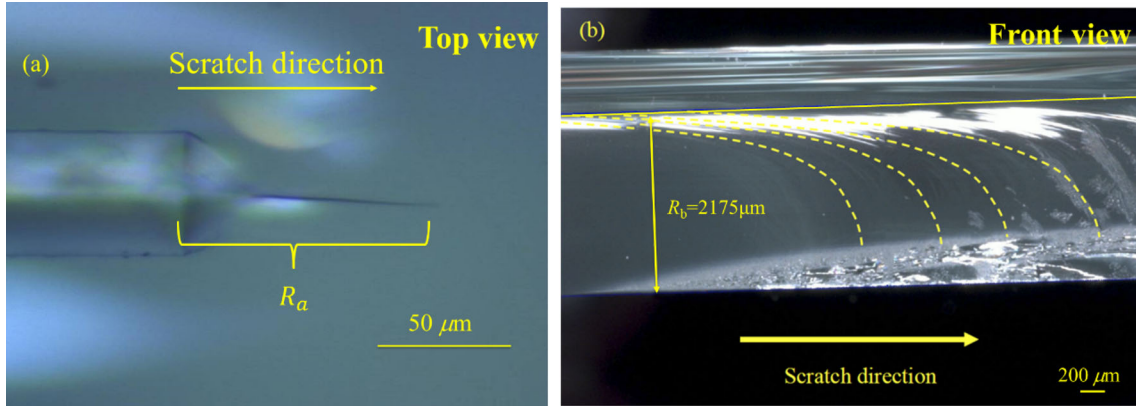
Fig. 7. **a** Confocal laser scanning microscopy image of a scratched-induced groove in soda-lime glass by a Vickers indenter under a normal load of 0.2 N and a scratch velocity of 2 mm/min; **b** longitudinal section of optical microscope of the crack along the scratch path for soda-lime glass
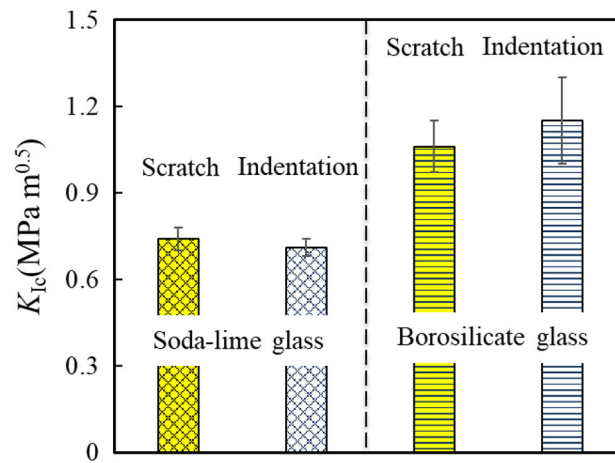

Fig. 8. Comparison of fracture toughness values of soda lime and borosilicate glasses obtained from indentation test and scratch test

borosilicate glasses, quartz glass has also been used to validate the proposed scratch-based method to characterize its fracture toughness. For the normal load, 0.097 N was used for quartz glass. The scratch velocity was 2 mm min^{-1}, and the scratch length was 5 mm. With E = 77.8 GPa, F_n = 0.098 N and R_b = 1.601 mm, it can be obtained $K_{Ic} = 0.68 \pm 0.10 \text{MPa}\sqrt{\text{m}}$, which is similar to the literature [44] using chevron-notched mirobeams. This reveals that the formula proposed in this paper is suitable to determine the fracture toughness of glasses.

4. Conclusion

A new formula is proposed to determine the fracture toughness of glasses via scratch tests using dimensional analysis and finite element analysis. The fracture toughness of glasses could be calculated with elastic modulus, crack depth of scratched materials and normal force applied during the scratch tests. The effect of plastic deformation and friction on determination of the fracture toughness of glasses cannot be neglected. The experimental verification of the formula on soda-lime and borosilicate glasses confirms that the proposed formula provides a convenient way to determine the fracture toughness of glasses.

References

[1] Cook R, Pharr G. Direct observation and analysis of indentation cracking in glasses and ceramics. J Am Ceram Soc. 1990;4:787–817. https://doi.org/10.1111/j.1151-2916.1990.tb05119.x.

[2] Anderson TL. Fracture mechanics: fundamentals and applications. Bona Raton: CRC Press; 2001.

[3] Bao C, Cai L, Shi K, et al. Improved normalization method for ductile fracture toughness determination based on dimensionless load separation principle. Acta Mech Solida Sin. 2015;25(2):168–81. https://doi.org/10.1016/S0894-9166(15)30005-7.

[4] Hong SH, Kim HY, Lee JR. Crack propagation behaviour during three-point bending of polymer matrix composite/Al2O3/polymer matrix composite laminated composites. Mat Sci Eng A - Struct. 1995;194:157–63. https://doi.org/10.1016/0921-5093(94)09677-5.

[5] To T, Célarié F, Roux-Langlois C, et al. Fracture toughness, fracture energy and slow crack growth of glass as investigated by the Single-Edge Precracked Beam (SEPB) and Chevron-Notched Beam (CNB) methods. Acta Mater. 2018;146:1–11. https://doi.org/10.1016/j.actamat.2017.11.056.

[6] Bao C, Cai LX. Investigation on compliance rotation correction for compact tensile specimen in unloading compliance method. Acta Mech Solida Sin. 2011;24(2):144–52. https://doi.org/10.1016/S0894-9166(11)60016-5.

[7] Lawn B, Wilshaw R. Indentation fracture: principles and applications. J Mat Sci. 1975;10:1049–81.

[8] Malzbender J, den Toonder JMJ, Balkenende AR, et al. Measuring mechanical properties of coatings: a methodology applied to nano-particle-filled sol-gel coatings on glass. Mat Sci Eng R. 2002;36:47–103.

[9] Zhao MH, Yang F, Zhang TY. Delamination buckling in the microwedge indentation of a thin film on an elastically deformable substrate. Mech Mater. 2007;39:881–92. https://doi.org/10.1016/j.mechmat.2007.03.003.

[10] Quinn GD, Bradt RC. On the Vickers indentation fracture toughness test. J Am Ceram Soc. 2007;90:673–80. https://doi.org/10.1111/j.1551-2916.2006.01482.x.

[11] Rickhey F, Marimuthu KP, Lee JH, et al. Evaluation of the fracture toughness of brittle hardening materials by Vickers indentation. Eng Fract Mech. 2015;148:134–44. https://doi.org/10.1016/j.engfracmech.2015.09.028.

[12] Ma DJ, Sun L, Wang LZ, et al. A new formula for evaluating indentation toughness in ceramics. Exp Mech. 2018;58:177–82. https://doi.org/10.1007/s11340-017-0325-8.

[13] Evans AG, Charles EA. Fracture toughness determinations by indentation. J Am Ceram Soc. 1976;59:371–2. https://doi.org/10.1111/j.1151-2916.1976.tb10991.x.

[14] Lawn BR, Evans AG, Marshall DB. Elastic/plastic indentation damage in ceramics: the median/radial crack system. J Am Ceram Soc. 1980;63:574–81. https://doi.org/10.1111/j.1151-2916.1980.tb10768.x.

[15] Feng Y, Zhang T, Yang R. A work approach to determine Vickers indentation fracture toughness. J Am Ceram Soc. 2011;94:332–5. https://doi.org/10.1111/j.1551-2916.2010.04289.x.

[16] Feng Y, Zhang T. Determination of fracture toughness of brittle materials by indentation. Acta Mech Solida Sin. 2015;28(3):221–34. https://doi.org/10.1016/S0894-9166(15)30010-0.

[17] Ostojic P, Mcpherson R. A review of indentation fracture theory: its development, principles and limitations. Int J Fract. 1987;33(4):297–312. https://doi.org/10.1007/BF00044418.

[18] Jiang H, Browning R, Sue HJ. Understanding of scratch-induced damage mechanisms in polymers. Polymer. 2009;50:4056–65. https://doi.org/10.1016/j.polymer.2009.06.061.

[19] Jiang H, Zhang J, Yang Z, et al. Modeling of competition between shear yielding and crazing in amorphous polymers' scratch. Int J Solids Struct. 2017;124:215–28. https://doi.org/10.1016/j.ijsolstr.2017.06.033.

[20] Zhang J, Jiang H, Jiang C, et al. Experimental and numerical investigations of evaluation criteria and material parameters' coupling effect on polypropylene scratch. Polym Eng Sci. 2018;58:118–22. https://doi.org/10.1002/pen.24538.

[21] Bull SJ, Berasetegui EG. An overview of the potential of quantitative coating adhesion measurement by scratch testing. Tribol Int. 2006;39:99–114. https://doi.org/10.1016/j.triboint.2005.04.013.

[22] Holmberg K, Laukkanen A, Ronkainen H, et al. A model for stresses, crack generation and fracture toughness calculation in scratched TiN-coated steel surfaces. Wear. 2003;254:278–91. https://doi.org/10.1016/S0043-1648(02)00297-1.

[23] Blackman BRK, Hoult T, Patel Y, et al. Steady-state scratch testing of polymers. Polym Test. 2016;49:38–45. https://doi.org/10.1016/j.polymertesting.2015.11.002.

[24] Wakeel SA, Hubler MH. Introducing heterogeneity into the micro-scratch test fracture toughness relation for brittle particle composites. Exp Mech. 2018;58:1237–47. https://doi.org/10.1007/s11340-018-0408-1.

[25] Subhash G, Loukus JE, Pandit SM. Application of data dependent systems approach for evaluation of fracture modes during a single-grit scratching. Mech Mater. 2002;34:25–42. https://doi.org/10.1016/S0167-6636(01)00083-7.

[26] Cook RF. Fracture mechanics of sharp scratch strength of polycrystalline alumina. J Am Ceram Soc. 2017;100:1146–60. https://doi.org/10.1111/jace.14634.

[27] Liu HT, Zhao MH, Zhang JW. Fracture properties of surface modification layers via a modified bi-layer beam model. J Mech. 2019;35:499–511. https://doi.org/10.1017/jmech.2018.36.

[28] Akono A, Reis PM, Ulm F. Scratching as a fracture process: from butter to steel. Phys Rev Lett. 2011;106:20430220. https://doi.org/10.1103/PhysRevLett.106.204302.

[29] Akono A, Ulm F. Scratch test model for the determination of fracture toughness. Eng Fract Mech. 2011;78:334–42. https://doi.org/10.1016/j.engfracmech.2010.09.017.

[30] Lin J, Zhou Y. Can scratch tests give fracture toughness? Eng Fract Mech. 2013;109:161–8. https://doi.org/10.1016/j.engfracmech.2013.06.002.

[31] Liu M, Yang S, Gao C. Scratch behavior of polycarbonate by Rockwell C diamond indenter under progressive loading. Polym Test. 2020;90:106643. https://doi.org/10.1016/j.polymertesting.2020.106643.

[32] Zhang D, Sun Y, Gao C, Liu M. Measurement of fracture toughness of copper via constant-load microscratch with a spherical indenter. Wear. 2020;444–445:203158. https://doi.org/10.1016/j.wear.2019.203158.

[33] Liu HT, Zhao MH, Lu CS, et al. Characterization on the yield stress and interfacial coefficient of friction of glasses from scratch tests. Ceram Int. 2020;46:6060–6. https://doi.org/10.1016/j.ceramint.2019.11.065.

[34] Wang W, Yao P, Wang J, et al. Elastic stress field model and micro-crack evolution for isotropic brittle materials during single grit scratching. Ceram Int. 2017;43:10726–36. https://doi.org/10.1016/j.ceramint.2017.05.054.

[35] Sani G, Limbach R, Dellith J, et al. Surface damage resistance and yielding of chemically strengthened silicate glasses: from normal indentation to scratch loading. J Am Ceram Soc. 2021. https://doi.org/10.1111/jace.17758.

[36] Matsuoka J, Guo D, Yoshida S. Cross-section morphology of the scratch-induced cracks in Soda-lime-silica glass. Front Mater. 2017;4:8. https://doi.org/10.3389/fmats.2017.00008.

[37] Shah RC, Kobayashi AS. Effect of poisson's ratio on stress intensity magnification factor. Int J Fract. 1973;9:360–1. https://doi.org/10.1007/BF00049223.

[38] Konda N, Erdogan F. The mixed mode crack problem in a nonhomogeneous elastic medium. Eng Fract Mech. 1994;47:533–45. https://doi.org/10.1016/0013-7944(94)90253-4.

[39] Lacroix R, Kermouche G, Teisseire J, et al. Plastic deformation and residual stresses in amorphous silica pillars under uniaxial loading. Acta Mater. 2012;60:5555–66. https://doi.org/10.1016/j.actamat.2012.07.016.

[40] Lin JS, Zhou Y. Rebuttal: shallow wide groove scratch tests do not give fracture toughness. Eng Fract Mech. 2015;133:211–22. https://doi.org/10.1016/j.engfracmech.2014.10.030.

[41] Anstis GR, Chantikul P, Lawn BR, et al. A critical evaluation of indentation techniques for measuring fracture toughness: I, direct crack measurements. J Am Ceram Soc. 1981;64:533–8.

[42] Iwata K, Tonegawa A, Nishi Y. Reduce brittleness of borosilicate glass by electron beam irradiation. J Jpn I Met. 2005;69:380–4. https://doi.org/10.2320/jinstmet.69.380.

[43] Gong J, Chen Y, Li C. Statistical analysis of fracture toughness of soda-lime glass determined by indentation. J Non-Cryst Solids. 2001;279:219–23. https://doi.org/10.1016/S0022-3093(00)00418-X.

[44] Mueller MG, Pejchal V, Zagar G, et al. Fracture toughness testing of nanocrystalline alumina and fused quartz using chevron-notched microbeams. Acta Mater. 2015;85:385–95. https://doi.org/10.1016/j.actamat.2014.12.016.